Research Article

Journal of Physical Organic Chemistry

Received: 13 March 2008, Revised: 16 July 2008, Accepted: 16 July 2008, Published online in Wiley InterScience: 26 August 2008

(www.interscience.wiley.com) DOI 10.1002/poc.1431

What governs nitrogen configuration in substituted aminophosphines?

Matthew D. Wodrich[a], Alfredo Vargas[b], Pierre-Yves Morgantini[b], Gabriel Merino[c] and Clémence Corminboeuf[a]*

The trigonal planar geometry of the nitrogen atom in commonly used phosphoramidite ligands is not in line with the traditional valence shell electron pair repulsion (VSEPR) model. In this work, the effects governing nitrogen configuration in several substituted aminophosphines, A_2PNB_2 (A or B = H, F, Cl, Br, Me, OMe, BINOP), are examined using modern computational analytic tools. The electron delocalization descriptions provided by both electron localization function (ELF) and block localized wavefunction analysis support the proposed relationships between conformation and negative hyperconjugative interactions. In the parent H_2PNH_2, the pyramidal nitrogen configuration results from nitrogen lone pair electron donation into the σ^* P—H orbital. While enhanced effects are seen for F_2PNMe_2, placing highly electronegative fluorine substituents on nitrogen (i.e., Me_2PNF_2) eliminates delocalization of the nitrogen lone pair. Understanding and quantifying these effects can lead to greater flexibility in designing new catalysts. Copyright © 2008 John Wiley & Sons, Ltd.

Keywords: stereoelectronic effects; electron delocalization; hyperconjugation; density functional theory

INTRODUCTION

Chiral phosphoramidite ligands widely used in asymmetric synthesis[1–13] (Fig. 1) possess a nitrogen atom in a trigonal planar conformation. Although this planarity may appear counter-intuitive, and in disagreement with the valence shell electron pair repulsion (VSEPR) model,[14] it is directly related to the electronic properties of the neighboring phosphorus atom and the Lewis acidity of the substituent. In the context of enantioselective catalysis, the experimental emphasis is generally placed on the chirality (**L1**) or atropoisomerism (fixed, i.e., **L2** or induced, i.e., **L3**) of the phosphorous group as well as on the modification of the amino functionality. However, understanding the stereoelectronic effects that govern nitrogen configuration is also of great interest for ligand design.

Atoms possessing lone-pairs of electrons are known to prefer structures where favorable orbital orientations allow for delocalization of the electron lone pair into an energetically low-lying σ^* orbital. These orbital interactions govern, for instance, the conformational preference of α-glucosides over ß-glucosides and are collectively known as the anomeric effect, the generalized anomeric effect, or negative hyperconjugation.[15–22] In an α-glucoside, the electron density is donated from the ring oxygen lone pair to the σ^* orbital between the carbon atom and the polar oxygen atom. This favorable interaction is maximized when the recipient σ^* orbital is in the axial position, thus α-glucosides are preferred energetically over ß-glucosides. However, this type of interaction exists not only in glucosides but are prevalent throughout chemistry. Roberts *et al.*[23] first used negative hyperconjugation (also referred to as double-bond no-bond resonance) to explain electrical effects in trifluoromethyl groups. Dewar examined negative hyperconjugation ($p_\pi \rightarrow d_\pi$ bonding) and other stereochemical factors influencing the P—N rotational barrier in aminophosphines.[24–27] Negative hyperconjugation has also been used to explain conformational preferences of fluoroalkyl groups, fluoroamines,[28] aminoborane,[29,30] alkyl-lithium complexes,[31] phosphazenes,[32,33] and pyridinium methylides,[34,35] to name only a few. In this paper, recent computational methodologies are used to examine the role of lone-pair delocalization and other stereoelectronic effects that establish nitrogen planarity in aminophosphines and phosphoramidite ligands.

COMPUTATIONAL METHODOLOGIES

Computations employing the hybrid-GGA density functional B3LYP[36,37] and second order Møller–Plesset perturbation theory (MP2)[38] were performed with the 6-31G(d),[39,40] 6-311+G(d,p),[41,42] 6-311++G(3df,3pd),[43,44] DZ,[45,46] DZP,[45–47] cc-pVDZ,[48] and cc-pVTZ[48] basis sets, using Gaussian03[49] and GAMESS-US.[50,51] Stationary points were characterized as minima on the corresponding potential energy surfaces by vibrational analysis at the same levels.

* *Correspondence to: C. Corminboeuf, Institut des Sciences et Ingénierie Chimiques, Ecole Polytechnique Fédérale de Lausanne (EPFL), Batochime, CH-1015, Lausanne, Switzerland.*
E-mail: clemence.corminboeuf@epfl.ch

a *M. D. Wodrich, C. Corminboeuf*
Institut des Sciences et Ingénierie Chimiques, Ecole Polytechnique Fédérale de Lausanne (EPFL), Batochime, CH-1015, Lausanne, Switzerland

b *A. Vargas, P-Y. Morgantini*
Département de Chimie Physique, Université de Genève, 30, quai Ernest-Ansermet, CH-1211 Geneva 4, Switzerland

c *G. Merino*
Facultad de Química, Universidad de Guanajuato, Noria Alta s/n CP 36050, Guanajuato, Guanajuato, Mexico

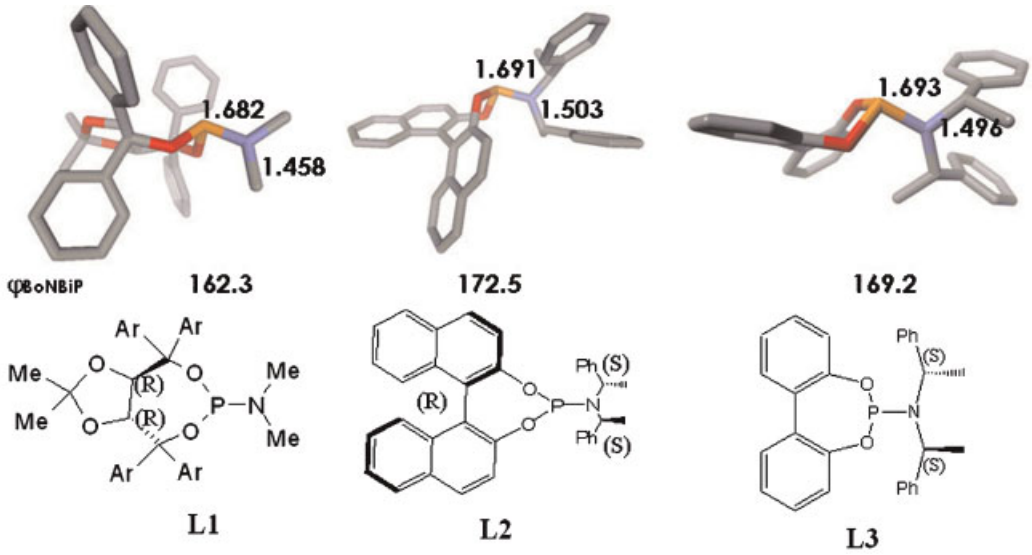

Figure 1. Examples of widely used phosphoramidite ligands[1,2,3] derived from secondary amine.[79] Geometrical parameters are given at the B3LYP/6-31G(d) level. Hydrogen atoms do not appear for clarity. This figure is available in colour online at www.interscience.wiley.com/journal/poc

The electron localization function (ELF) was analyzed with the TopMod[52] program using density matrices obtained from Gaussian orbital computations. The ELF, which was introduced by Becke and Edgecombe as a 'simple measure of electron localization in atomic and molecular systems'[53,54] is defined as:

$$\mathrm{ELF}(\mathbf{r}) = \left(1 + \frac{t(\mathbf{r})}{t_h(\mathbf{r})}\right)^{-1}$$

It is a useful tool which provides deeper insight into the nature of the chemical bonding in a variety of stationary and reacting systems. ELF(**r**) can be conveniently written (and interpreted) for monodeterminantal wavefunctions in terms of the excess of local kinetic energy density arising from the Pauli repulsion, $t(\mathbf{r})$, with the Thomas–Fermi kinetic energy density, $t_h(\mathbf{r})$, chosen as a reference. Hence, $\mathrm{ELF}(\mathbf{r}) = 0$ in those regions where the relative probability of finding electrons with parallel spin close together is high (i.e., where the local Pauli repulsion is strong), whereas $\mathrm{ELF}(\mathbf{r}) = 1$ in those regions with a high probability of finding a single electron or a pair of opposite spin electrons. The analysis of the ELF gradient field, $\bigtriangledown\mathrm{ELF}(\mathbf{r})$, provides a division of the molecular space into basins of attractors (i.e., maxima), which can be thought of as corresponding to atom core, valence, bonding, and non-bonding regions. There is, in principle a one-to-one correspondence between the VSEPR electronic domains and the valence basins of the ELF function. Indeed, the VSEPR model relies on a distribution of the valence electron pairs among bonding and nonbonding electron domains,[55] which are defined as the region of space in which the probability of finding an (opposite spin) electron pair is high. In the ELF analysis, the valence basins are characterized by the number of atomic valence shells in which they participate. This number is called a synaptic order and includes, for instance, mono- and di-synaptic basins, etc. Monosynaptic basins, labeled V(A), correspond to the lone pair of the Lewis acid model. Disynaptic basins, labeled V(A,X), correspond to two-center bonds, etc. The hierarchy of the basins is reflected in tree-diagrams (or bifurcation diagrams) that are built based on the ELF values at critical points located on the separatrix between two basins (i.e., the separation between the different localization domains). The higher the separation (bifurcation) value, the higher the expected degree of delocalization of electron pairing between these domains.[56]

The geometric and energetic effects of π-electron delocalization are measured using the block-localized wavefunction (BLW) approach of Mo *et al.*[57,58] BLW is a molecular orbital-based procedure for obtaining valence bond quantities that represents a unique approach for probing electron delocalization in chemical systems. It allows for the localization of electrons in specific regions of the molecular system, which may, for example, include 2π electrons in a C═C bond, or an electron lone pair. The wavefunction and geometries of these localized structures can then be optimized at the DFT level, allowing for the direct assessment of the geometric and energetic effects resulting from electron delocalization. This procedure has previously been incorporated in studies of the unusually short C—C bond in tetrahedranyltetrahedrane[59] as well as to study the roles of negative hyperconjugation ($n \rightarrow \sigma^*$), $p_\pi \rightarrow d_\pi$ bonding, and stereoelectronic interactions in trisilylamine.[60] Here, we compare the BLW-B3LYP/6-311 + G(d,p) and B3LYP/6-311 + G(d,p) geometries and energies to analyze the effects associated with nitrogen and phosphorus lone pair delocalization. The larger phosphoramidite ligands were optimized at both the B3LYP/6-31G(d) and B3LYP/3-21G level, with both basis sets giving the same geometrical trends. Due to technical limitations, BLW computations on these ligands are performed only at the BLW-B3LYP/3-21G level and compared to the B3LYP/3-21G geometries (*vide infra*).

RESULTS AND DISCUSSION

Previous theoretical studies on aminophosphines have debated the structure of the parent aminophosphine, H_2PNH_2,[33,61–69] which is known to favor an orthogonal pyramidal configuration by ~5 kcal mol^{-1} over the antipyramidal structure (as shown in Figs 2 and 3).[70] Early studies on this parent compound also highlighted the importance of using basis sets possessing polarization functions,[68] which are necessary on both phosphorus and nitrogen atoms to obtain the correct molecular

Journal of Physical Organic Chemistry

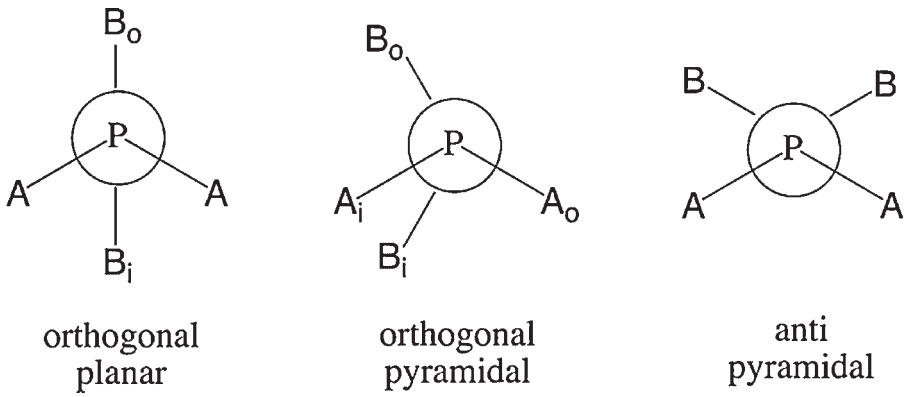

Figure 2. Nomenclature used in the text for the conformations of the nitrogen and phosphorous substitutents, that is A/B_i or A/B_0 refer to *inner* and *outer* substituents. The same nomenclature as in Reference [60] is used

geometry. A key characteristic geometrical feature is the $\varphi(B_iNPB_0)$ dihedral angle, a measure of pyramidality of the nitrogen atom. With the exception of the Dunning DZ (which predicts a planar nitrogen structure), all basis sets predict a pyramidal configuration for nitrogen, with values ranging from 121 to 136° (as shown in Table 1). Also, the same overall trends are given by both MP2 and B3LYP.

To clearly understand the preference of H_2PNH_2 for the ortho pyramidal configuration (Fig. 2), the geometries, and energies of several aminophosphines with distinct substituents have been investigated. Methyl and halogen substituents have been chosen based on their contrasting electronic properties. Replacement of the hydrogen atoms in H_2PNH_2 (**1**) with halogens and methyl groups (i.e., X_2PNMe_2 and Me_2PNX_2 (X = F, Cl, Br)) alters the pyramidality (the $\varphi(B_iNPB_0)$ dihedral angle) of the substituted aminophosphine.

For instance, in all X_2PNMe_2 aminophosphines the nitrogen atom pyramidality is smaller (more planar) than in **1** (Table 2 and Fig. 3). In contrast, when halogens are bonded directly to nitrogen, its pyramidality is greatly enhanced (less planar). Fluorine produces the most dramatic change in pyramidality between F_2PNMe_2 (**2**) and Me_2PNF_2 (**3**) (from 174.2° in **2** to 108.3° in **3**). While the emphasis is first placed on the two limiting cases **2** and **3** along with the parent molecule **1**, further analysis are provided on a representative phosphoramidite ligand and its derivatives.

H_2PNH_2 (1)

The topological analysis of ELF provides a clear picture of bonding that can be rationalized through the analysis of basin bifurcations (i.e., separation, shown above). Figure 4 shows the ELF isosurface for **1**. As expected, this system is characterized by the presence of a disynaptic valence basin, V(P,N), together with two monosynaptic basins, V(P) and V(N), for the corresponding lone pairs. As displayed in the bifurcation diagram, the first separation occurs at the ELF critical value of 0.56, where the phosphorus region is separated from the rest of the system. The second bifurcation occurs at the ELF critical value of 0.77 for the domain associated to the P—H_0 bond. The later domain is slightly more localized than that associated with the P—H_i bond. This small difference as well as variation between the P—A_i and P—A_0 bond lengths in **1** suggest a significant delocalization of the nitrogen lone pair into the σ^* P—A_i orbital (as shown in orbital scheme on Fig. 3). Such anomeric effect stabilizes the pyramidal form and explains the elongation of the P—A_i bond length with respect to P—A_0 (1.434 *vs.* 1.423 Å, Table 2). Note that the ELF tree-diagram also shows that the nitrogen lone pair is clearly more delocalized than the phosphorus lone pair.

In addition to the geometrical parameters and the ELF analysis, useful insights can be provided using the block localized wavefunction method. The latter approach is used to directly quantify and further rationalize the effect of electron delocalization influencing nitrogen planarity in the limit cases **1**, **2**, and **3**. The geometric and energetic influences of electron delocalization can be evaluated by comparing the geometry and energy of the BLW-B3LYP diabatic states where the nitrogen lone pair is forbidden from delocalization with the B3LYP adiabatic state (where the N lone pair is delocalized). The constrained localization of the nitrogen lone pair in **1** leads to significant structural variation. In the diabatic state, the electron lone pair of the nitrogen atom is strictly localized and the N—P bond is thus a 'pure' N(sp^2)—P(sp^3) single bond. Consequently, the P—N bond length is significantly longer (by 0.03 Å) and the P—A_i shorter (by 0.01 Å) than in the adiabatic state. Energetically, the delocalization energy of the nitrogen lone pair in **1** is slightly superior to 10 kcal mol^{-1}, a magnitude similar to the conventional (positive) hyperconjugation in propene, which has been recently investigated with the same methodology.[57,71]

F_2PNMe_2 (2)

F_2PNMe_2 has a nearly planar nitrogen atom and a double bond like character for the P—N bond (Table 2, 1.663 Å). The ELF isosurface for **2** is typical (as shown in Fig. 4) of sp^2-atom containing molecules with the presence of two V(N) basins, one above and one below the nitrogen core.[72] The planar symmetry at the nitrogen indeed implies that the probability of finding a basin above the plane be matched by an equal probability below the plane. The bifurcation diagram, which gives the critical value related to the partition of the V(N) and V(P,N) domains indicates that the nitrogen lone pair in **2** (0.88) is more delocalized than that in **1** (0.86). These enhanced delocalization associated with the short P—N bond, clearly support a negative hyperconjugative interaction from the nitrogen lone pair into a three-center antibonding σ_{XPX} orbital (Fig. 3). The immediately consequences is a large lone pair delocalization energy (~30 kcal mol^{-1} at the BLW-B3LYP/6-311 + G** level). This interaction, previously discussed in Reference [69] favors the planar configuration, and is triggered by the strongly attracting phosphorous substituents.

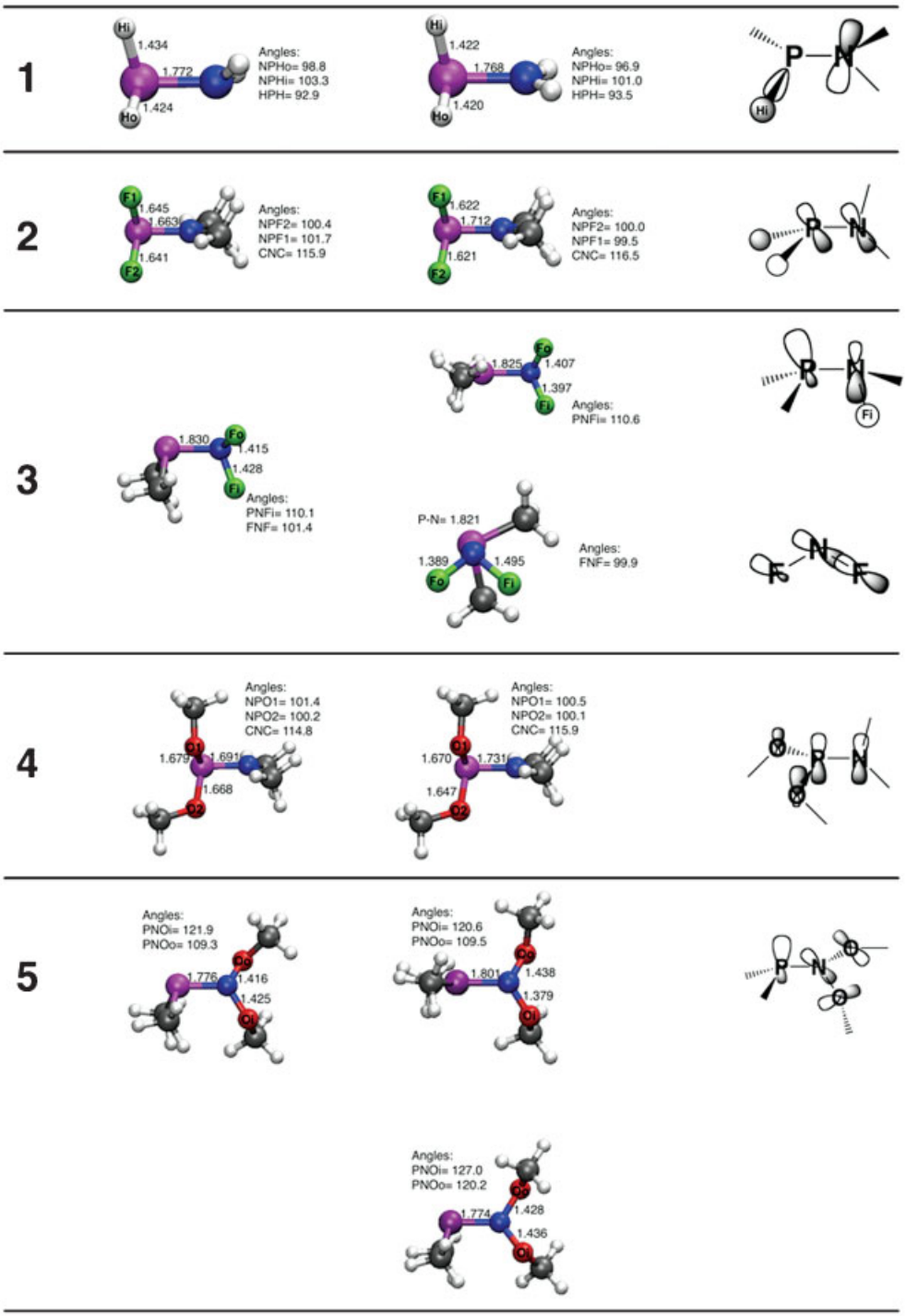

Figure 3. Left: structures and geometrical parameters at the B3LYP/6-311 + G(d,p) level of H_2PNH_2 (**1**), F_2PNMe_2 (**2**) Me_2PNF_2 (**3**), $(MeO)_2PNMe_2$ (**4**), and $Me_2PN(OMe)_2$ (**5**). Middle: BLW-B3LYP/6-311 + G(d,p) geometries for **1**, **2**, **4** (nitrogen lone pair blocked), **3** (lone pair of F_i blocked, top; lone pair of phosphorous blocked, bottom), and **5** (lone pair of the phosphorous blocked). Right: schematic representation of the representative molecular orbital interactions in **1**, **2**, **3**, **4**, and **5**

The evidence for such $n_N \rightarrow \sigma^*_{FPF}$ negative hyperconjugation also challenges the concept of p_π—d_π bonding as initially proposed to explain the planar structures of silylamines.[73–76] In the localized structure (Fig. 3), the localization of the nitrogen lone pair increases the P—N bond by 0.044 Å and significantly shortens the P—F bonds as expected in the case of a $n_N \rightarrow \sigma^*_{FPF}$ interactions. Cl_2PNMe_2 and Br_2PNMe_2 are also characterized by a short P—N bond (Table 2) however, the nitrogen atom shows a larger deviation from planarity.

Me_2PNF_2 (3)

In the molecule with the opposite groups coordinated to the nitrogen and phosphorous atoms, the long P—N bond length

Table 1. Relevant bond length (in angstrom) and dihedral angle (in degrees) indicating the pyramidality of nitrogen atom in H_2PNH_2 at B3LYP and MP2 with different size basis sets

		6-31G(d)	6-311 + G(d,p)	6-311++G(3df,3pd)	DZ	DZVP	cc-pVDZ	cc-pVTZ
P–N	B3LYP	1.727	1.723	1.711	1.753	1.717	1.747	1.721
	MP2	1.723	1.719	1.707	1.762	1.714	1.749	1.717
N–B_i	B3LYP	1.014	1.010	1.009	1.011	1.014	1.020	1.009
	MP2	1.014	1.010	1.008	1.014	1.012	1.021	1.008
N–B_0	B3LYP	1.013	1.009	1.007	1.009	1.012	1.019	1.008
	MP2	1.013	1.009	1.007	1.013	1.010	1.020	1.007
P–A_i	B3LYP	1.437	1.433	1.427	1.450	1.432	1.449	1.432
	MP2	1.425	1.418	1.415	1.443	1.413	1.435	1.420
P–A_0	B3LYP	1.424	1.423	1.418	1.450	1.421	1.436	1.421
	MP2	1.414	1.409	1.407	1.443	1.403	1.423	1.411
$\varphi(B_iNPB_0)$	B3LYP	131.9	139.7	137.5	180.0	138.2	124.6	133.1
	MP2	132.2	135.4	135.3	180.0	136.9	121.7	130.1

(1.830 Å) suggests that the nitrogen lone pair is not delocalized as in the previous cases. Figure 4 illustrates also the topology of the ELF domains for **3**. Clearly, the organization of attractors around the nitrogen atom is similar to that in **1**. However, in the case of **3**, the ELF critical value related to the separation of the V(N) and V(P,N) domains (0.84) is lower than the corresponding value for **1** (0.86) indicating that the nitrogen lone pair in **3** is more localized than in **1** and **2**. In contrast, the critical value associated with V(P) is larger in **3** than in **2**.

Instead of the nitrogen lone pair delocalization, two competitive effects maximize the φ(FNPF) dihedral angle and the barrier to planarity (19.1 kcal mol^{-1} at the B3LYP/6-311 + G(d,p) level): (i) the favorable geminal fluorine–fluorine negative hyperconjugation interaction between the non-bonding electron pair on fluorine and the vacant σ^*-orbital of the adjacent N—F bond ($n_F \rightarrow \sigma^*_{NF}$, Fig. 3). Such anomeric effects are also known to stabilize methylene chloride and CH_2F_2[77] and are consistent with the significantly shorter N—B_0(=F) bond length (1.415 Å in Table 2) as compared to NFH_2 (1.433 Å at the same level). (ii) The second effect involves an increase in phosphorus lone pair delocalization ($n_P \rightarrow \sigma^*_{NB_i=F}$) in comparison with **2** resulting in a deviation between N—B_i and N—B_0 bond. Two localized structures (Fig. 3) with respectively the lone pair of the fluorine and phosphorus atoms blocked illustrate these cooperative effects resulting in the lengthening/shortening of the N—F_i (Fig. 3).

Phosphoramidite ligands

The above discussion on simple aminophosphines cannot be fully generalized to phosphoramidite ligands unless oxygen-containing substituents are considered. Thus, the replacement of the halogen atoms by methoxy groups such as in $(MeO)_2PNMe_2$ (**4**) and $Me_2PN(OMe)_2$ (**5**) represent a logical extension to **2** and **3**. Such a modification does not influence the main stereoelectronic trends significantly, and highlights the importance of the electronegativity of the substituent. In **4**, the electron delocalization of the nitrogen lone pair into the asymmetrical three-center antibonding σ^*_{OPO} orbital leads to intermediary electronic effects as compared to H_2PNH_2 (**1**) and F_2PNMe_2 (**2**): the φ(CNPC) dihedral angle (156.9°, Table 2) as well as the P—N bond length (1.691 Å) are in between the geometrical parameters of the two benchmark compounds. Similarly, the blocking of the nitrogen lone pair results in a slightly attenuated (or intensified)

Table 2. Geometrical parameters for $A_0A_iPNB_iB_0$ computed at B3LYP/6-311 + G(d,p)

		$A_iA_0PNMe_2$			$Me_2PNB_iB_0$						
	Parent A=B=H **1**	A_i=A_0=Br[a]	=Cl	=F **2**	B_i=B_0=Br	=Cl	=F **3**	**4**	**5**	**L3**[a]	**L3′**
P–N	1.723	1.688	1.675	1.663	1.779	1.789	1.830	1.690	1.776	1.693	1.816
N–B_i	1.010	1.464	1.465	1.462	1.987	1.822	1.428	1.458	1.425	1.496	1.457
N–B_0	1.009	1.470	1.470	1.462	1.936	1.778	1.415	1.460	1.416	1.496	1.459
P–A_i	1.434	2.312	2.171	1.641	1.856	1.852	1.851	1.679	1.869	1.692	1.910
P–A_0	1.424	2.259	2.118	1.645	1.852	1.846	1.851	1.667	1.849	1.696	1.895
$\varphi(B_iPNB_0)$	139.3	146.9	152.9	174.2	121.2	123.9	108.3	156.9	134.1	169.2	120.6

Bond lengths are given in angstrom and dihedral angle in degrees.
[a] Br_2PNMe_2, Me_2PNBr_2, **L3**, and **L3′**computed at B3LYP/6-31G(d).

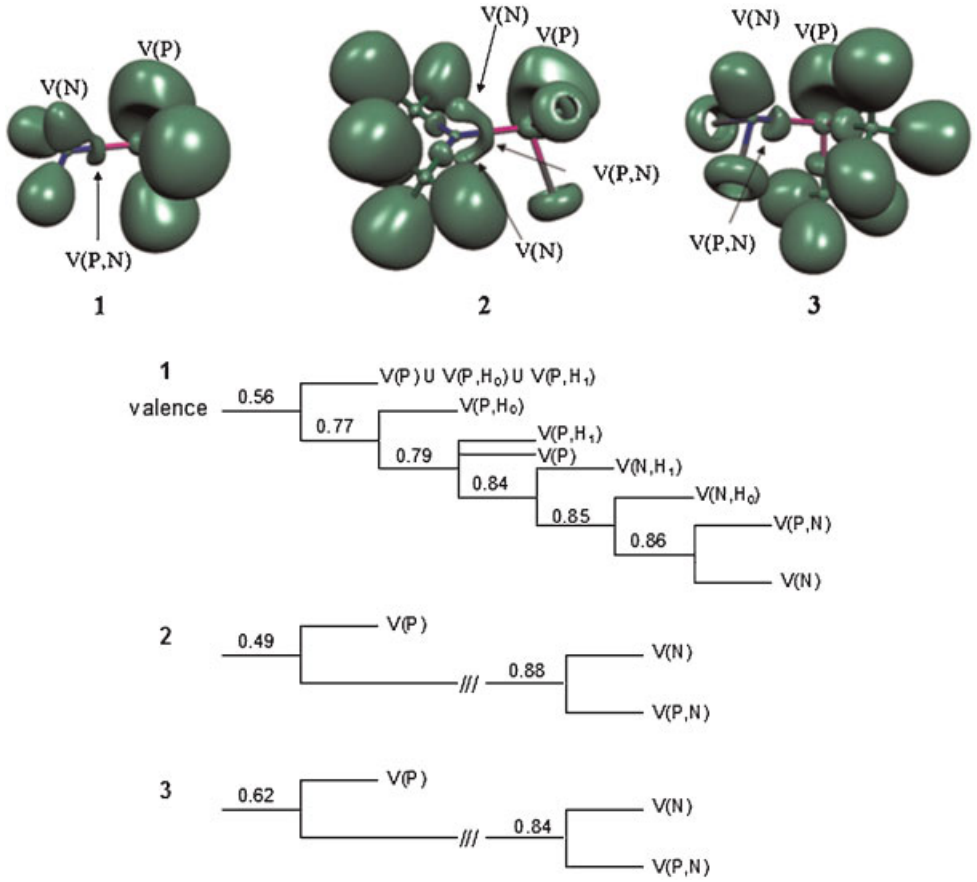

Figure 4. Top: graphical representation of the ELF localization domains for **1**, **2**, and **3**. The value of ELF is equal to 0.85. Bottom: corresponding ELF bifurcation diagrams. The critical value corresponds to the highest saddle point on the separatrix between the corresponding domains. For **2** and **3**, the diagrams depict only the critical points corresponding to the separation involving the most relevant basins V(N), V(P), and V(P,N)

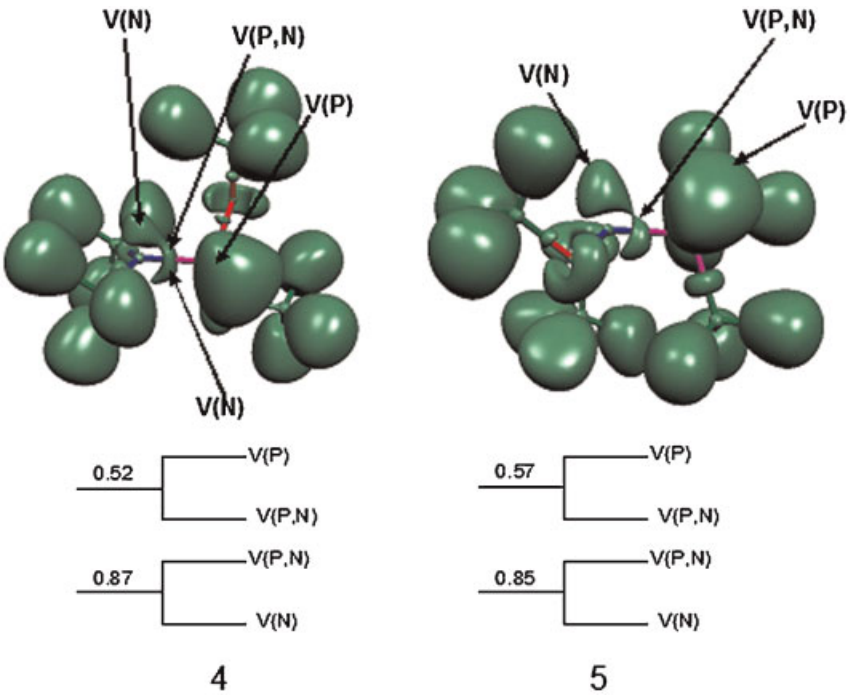

Figure 5. Top: graphical representation of the ELF localization domains for **4** and **5**. The value of ELF is equal to 0.85. Bottom: corresponding ELF bifurcation diagrams. The critical value corresponds to the highest saddle point on the separatrix between the corresponding domains. The diagrams depict only the critical points corresponding to the separation involving the most relevant basins V(N), V(P), and V(P,N)

Journal of Physical Organic Chemistry

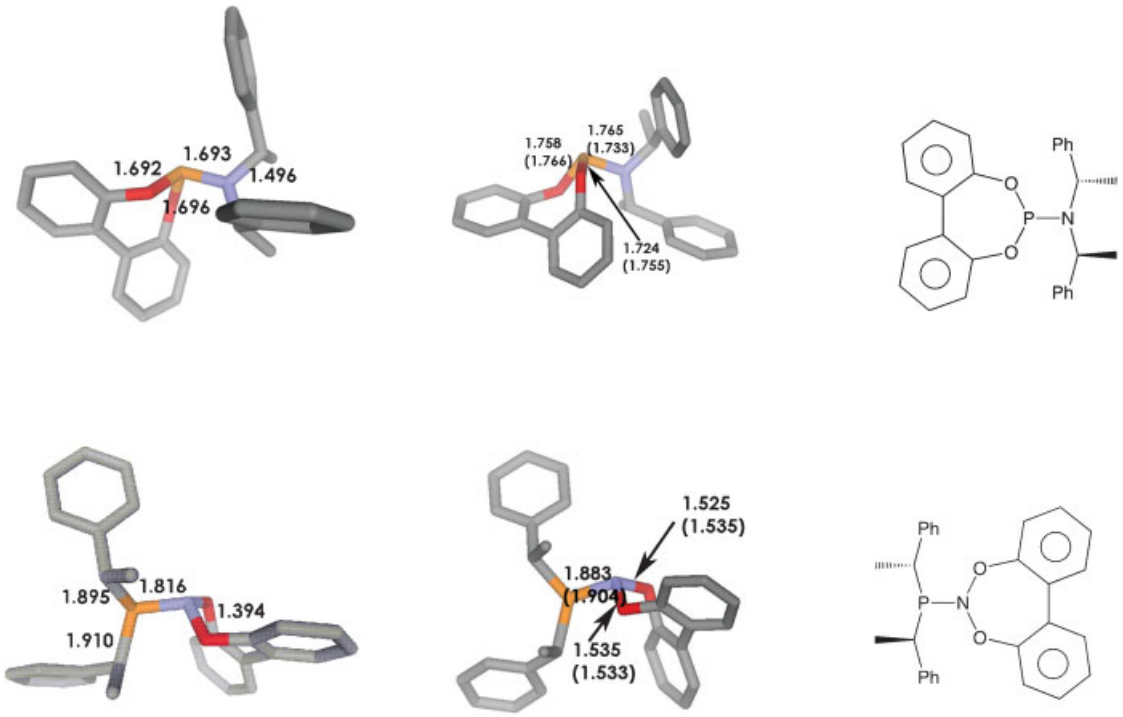

Figure 6. Left: structures and geometrical parameters of **L3** and **L3**′ (constitution isomer of **L3**) at the B3LYP/6-31G(d) level (bond lengths are given in Å). Middle: structures and geometrical parameters at BLW-B3LYP/3-21G for **L3** (nitrogen lone pair blocked) and **L3**′ (lone pair of phosphorous blocked). Since a smaller basis sets had to be used for the BLW optimization of **L3** and **L3**′, the B3LYP/3-21G geometrical parameters are given in parenthesis for comparison. Right: schematic representation

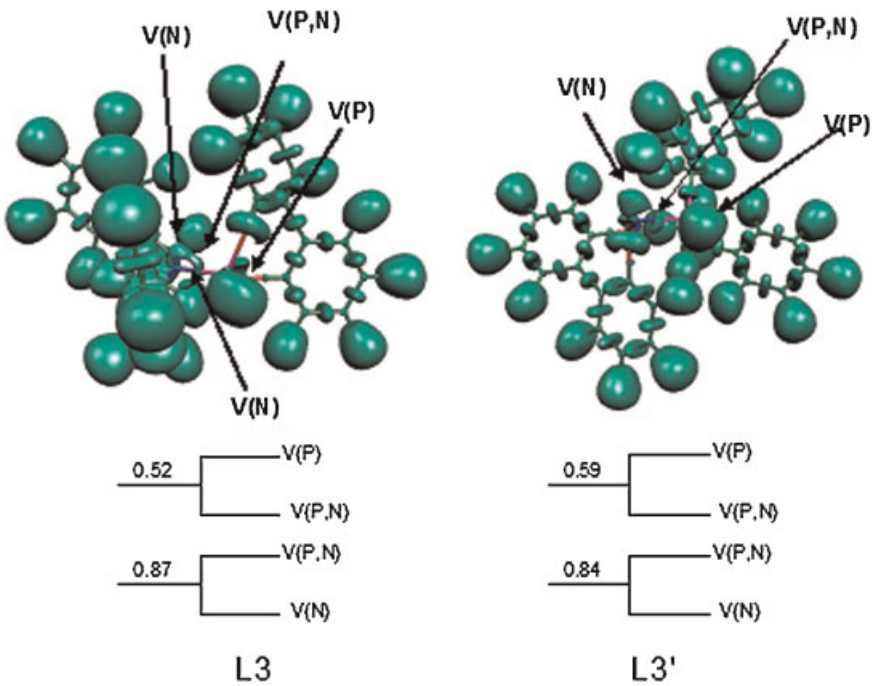

Figure 7. Top: graphical representation of the ELF localization domains for **L3**, and **L3**. The value of ELF is equal to 0.85. Bottom: corresponding ELF bifurcation diagrams. The diagrams depict only the critical points corresponding to the separation involving the most relevant basins V(N), V(P), and V(P,N)

lengthening of the P—N bond (0.04 Å) and shortening of the two P—O bond lengths (0.021 and 0.009 Å) as compared to **2** (or **1**) (Fig. 3). Finally, the bifurcation diagram of **4** also gives intermediary critical values for the V(P), V(N), and V(P,N) as compared to **1** and **2** (Fig. 5).

In sharp contrast, the geometrical parameters in **5** are reminiscent of **3** with a long P—N bond length (1.776 Å) and a pyramidal nitrogen (φ(FNPF) = 134°) suggesting that the nitrogen lone pair is not delocalized into the phosphorous side. According to the ELF bifurcation diagram (Fig. 5), the phosphorous and nitrogen lone pairs are respectively more and less delocalized than in **4**. The BLW data further indicates that the nitrogen lone pair interacts with the oxygen lone pairs rather than with the phosphorous side. Consequently, the blocking of the nitrogen lone pair in **5** only marginally affects the length of the P—N and P—C bonds but significantly alters the N—O bond lengths (Fig. 3). Akin to **3**, the delocalization of the phosphorous lone pair into the nitrogen side ($n_P \rightarrow \sigma^*_{N-OMe}$) results in a deviation between N—B_i and N—B_0 bond.

From the electronic point of view, the phosphoramidites ligands commonly used in catalysis (e.g., **L1**, **L2**, and **L3**, shown in Figs. 1 and 6) are more like **2** and **4** with the electron withdrawing groups on the phosphorous enhancing the $n_N \rightarrow \sigma^*_{XPX}$ negative hyperconjugation and enforcing both the planar configuration of the nitrogen atom (>160°) as well as the double-bond character of the P—N bond length (<1.695 Å, Fig. 1). These effects can be further demonstrated by the blocking of the nitrogen lone pair in, for instance, **L3** resulting in a significant increase of the P—N bond distance and shortening of the P—O bond lengths. Also, the ELF bifurcation values for the V(P), V(N), and V(P,N) domains are the same as for **4** (Fig. 7).

Unsurprisingly, contrasting trends are obtained for the constitution isomer **L3′** having the π-attractor BINOP-derivative bonds to nitrogen instead of phosphorous and reciprocally for the nitrogen electron-donating substituents. In line with the trends observed for the compound **5**, **L3′** has a pyramidal nitrogen atom ($\varphi_{B_0NB_iP}$ = 120.58) and a much longer P—N bond length (1.816 Å) (Fig. 6) than **L3** (1.693 Å). The ELF analysis indicates that the phosphorous lone pair is more delocalized than in **L3** (Fig. 7), while the opposite trend is found for the nitrogen lone pair. These trends nicely illustrate that both the φ(RNPR) dihedral angle and the barrier to nitrogen planarity could be easily tuned by alternating the substituents. While the use of such ligands with the electron donating groups coordinated to phosphorous rather than nitrogen have never been used in catalysis, studies focusing on the fundamental electronic factors characterizing the phosphoramidite ligands and their constitution isomers remain undoubtfully important following the continuous interest in (stereoelectronic) ligand design.[78]

CONCLUSIONS

The stereoelectronic effects that control nitrogen configuration in aminophosphines and phosphoramidite ligands have been investigated and identified on three benchmark derivatives H_2NPH_2 (**1**), F_2PNMe_2 (**2**), and Me_2PNF_2 (**3**) using electronic structure theories. While the nitrogen configuration changes from pyramidal in both **1** and **3** to quasi-planar in **2**, both ELF and BLW analysis show that negative hyperconjugation interactions are largely responsible for determining the degree of nitrogen pyramidalization. Substitution of aminophosphines by less electronegative, heavier halogen atoms produces similar although less pronounced changes to nitrogen configurations to those with fluorine.

The alteration of functional groups also influences the negative hyperconjugative interactions as well as the nitrogen atom configuration in widely used phosphoramidite ligands and derivatives (e.g., MeO_2PNMe_2 (**4**) and Me_2PNMeO_2 (**5**)). The identification of the electronic factors governing the structure of such ligands is of primary importance for the design of novel catalysts.

Acknowledgements

We thank Alexandre Alexakis and Damien Polet for synthesizing an inspiring ligand (**L3**), and helpful discussions. Clemence Corminboeuf acknowledges the Sandoz Family Foundation and Gabriel Merino acknowledges the support from Conacyt (Grant 57892). The authors thank Professor Yirong Mo for making his program available.

REFERENCES

[1] R. Hulst, N. Koen de Vries, B. L. Feringa, *Tetrahedron: Asymmetry* **1994**, *5*, 699–708.
[2] J. F. Jensen, B. Y. Svendsen, T. V. la Cour, H. L. Pedersen, M. Johannsen, *J. Am. Chem. Soc.* **2002**, *124*, 4558–4559.
[3] L. A. Arnold, R. Imbos, A. Mandoli, A. H. M. de Vries, R. Naasz, B. L. Feringa, *Tetrahedron* **2000**, *56*, 2865–2878.
[4] B. L. Feringa, *Acc. Chem. Res.* **2000**, *33*, 346–353.
[5] B. Bartels, G. Helmchen, *Chem. Comm.* **1999**, 741–742.
[6] K. Fuji, N. Kinoshita, K. Tanaka, T. Kawabata, *Chem. Comm.* **1999**, 2289–2290.
[7] T. Ohmura, J. F. Hartwig, *J. Am. Chem. Soc.* **2002**, *124*, 15164–15165.
[8] A. Alexakis, S. Rosset, J. Allamand, S. March, F. Guillen, C. Benhaim, *Synlett.* **2001**, *9*, 1375–1378.
[9] D. Polet, A. Alexakis, *Org. Lett.* **2005**, *7*, 1621–1624.
[10] E. J. Zijp, J. I. van der Vlugt, D. M. Tooke, A. L. Spek, D. Vogt, *Dalton Trans.* **2005**, *3*, 512–517.
[11] D. Polet, A. Alexakis, K. Tissot-Croset, C. Corminboeuf, K. Ditrich, *Chem. Eur. J.* **2006**, *12*, 3596–3609.
[12] G. Helmchen, A. Dahnz, P. Dübon, M. Schelwies, R. Weihofen, *Chem. Comm.* **2007**, 675–691.
[13] K. Wakabayashi, K. Aikawa, S. Kawauchi, K. Mikami, *J. Am. Chem. Soc.* **2008**, *130*, 5012–5013.
[14] R. J. Gillespie, I. Hargittai, *The VSEPR Model of Molecular Geometry*, Allyn and Bacon, Needham Heights, **1991**.
[15] A. J. Kirby, *The Anomeric Effect and Related Stereoelectronic Effects at Oxygen*, Springer, New York, **1983**.
[16] W. A. Szarek, D. Horton, *Anomeric Effect*, American Chemical Society, Washington, **1979**.
[17] P. Deslongchamps, *Stereoelectronic Effects in Organic Chemistry*, Pergamon Elmsford, New York, **1983**. p. 4.
[18] N. S. Zefirov, *Tetrahedron* **1977**, *33*, 2719–2722.
[19] N. S. Zefirov, N. M. Shekhtman, *Russ. Chem. Rev.* **1971**, *40*, 315–329.
[20] R. U. Lemieux, *Pure Appl. Chem.* **1971**, *27*, 527–547.
[21] S. J. Angyal, *Angew. Chem. Int. Ed. Engl.* **1969**, *8*, 157–166.
[22] J. Martin, *Ann. Chem. (Paris)* **1971**, *6*, 205–218.
[23] J. D. Roberts, R. L. Webb, E. A. McElhill, *J. Am. Chem. Soc.* **1950**, *72*, 408–411.
[24] A. H. Cowley, M. J. S. Dewar, W. R. Jackson, *J. Am. Chem. Soc.* **1968**, *90*, 4185–4186.
[25] A. H. Cowley, M. J. S. Dewar, W. R. Jackson, W. B. Jennings, *J. Am. Chem. Soc.* **1970**, *92*, 1085–1086.
[26] A. H. Cowley, M. J. S. Dewar, W. R. Jackson, W. B. Jennings, *J. Am. Chem. Soc.* **1970**, *92*, 5206–5213.
[27] A. H. Cowley, M. J. S. Dewar, D. W. Goodman, J. R. Schweiger, *J. Am. Chem. Soc.* **1973**, *95*, 6506–6508.

[28] J. J. Urban, *J. Phys. Org. Chem.* **2005**, *18*, 1061–1071.
[29] B. L. Kormos, C. J. Cramer, *Inorg. Chem.* **2003**, *42*, 6691–6670.
[30] Y. Mo, S. D. Peyerimhoff, *Theor. Chem. Acc.* **1999**, *101*, 311–318.
[31] W. Scherer, P. Sirsch, D. Shorokhov, G. S. McGrady, S. A. Mason, M. G. Gardiner, *Chem. Eur. J.* **2002**, *8*, 2324–2334.
[32] R. Murugavel, S. S. Krishnamurthy, J. Chandrasekhar, M. Nethaji, *Inorg. Chem.* **1993**, *32*, 5447–5453.
[33] A. B. Chaplin, J. A. Harrison, P. J. Dyson, *Inorg. Chem.* **2005**, *44*, 8407–8417.
[34] N. Gupta, K. K. Shah, R. Garg, *J. Org. Chem.* **2006**, *71*, 1344–1350.
[35] R. K. Bansal, N. Gupta, S. Singh, K. Karaghiosoff, P. Mayer, M. Vogt, *Tetrahedron Lett.* **2004**, *45*, 7771–7773.
[36] A. D. Becke, *J. Chem. Phys.* **1993**, *98*, 5648–5652.
[37] C. T. Lee, W. T. Yang, R. G. Parr, *Phys. Rev. B* **1998**, *37*, 785–789.
[38] C. Møller, M. S. Plesset, *Phys. Rev.* **1934**, *46*, 618–622.
[39] P. C. Hariharan, J. A. Pople, *Theoret. Chimica Acta* **1973**, *28*, 213–222.
[40] W. J. Hehre, R. Ditchfield, J. A. Pople, *J. Chem. Phys.* **1972**, *56*, 2257–2261.
[41] R. Krishnan, J. S. Binkley, R. Seeger, J. A. Pople, *J. Chem. Phys.* **1980**, *72*, 650–654.
[42] T. Clark, J. Chandrasekhar, Pv. R. Schleyer, *J. Comput. Chem.* **1983**, *4*, 294–301.
[43] A. D. McLean, G. S. Chandler, *J. Chem. Phys.* **1980**, *72*, 5639–5648.
[44] M. J. Frisch, J. A. Pople, J. S. Binkley, *J. Chem. Phys.* **1984**, *80*, 3265–3269.
[45] T. H. Dunning, *J. Chem. Phys.* **1970**, *53*, 2823–2833.
[46] T. H. Dunning, P. J. Hay, "Gaussian basis sets for molecular calculations" Chapter 1. in: *Electronic Structure Theory*, Vol. 3 (Ed.: H. F. Schaefer), Plenum, New York, **1977**.
[47] E. Magnusson, H. F. Schaefer, *J. Chem. Phys.* **1985**, *83*, 5721–5726.
[48] T. H. Dunning, *J. Chem. Phys.* **1989**, *90*, 1007–1023.
[49] 03. Gaussian, C02. Revision, M. J. Frisch, G. W. Trucks, H. B. Schlegel, G. E. Scuseria, M. A. Robb, J. R. Cheeseman, J. A. Montgomery, Jr., T. Vreven, K. N. Kudin, J. C. Burant, J. M. Millam, S. S. Iyengar, J. Tomasi, V. Barone, B. Mennucci, M. Cossi, G. Scalmani, N. Rega, G. A. Petersson, H. Nakatsuji, M. Hada, M. Ehara, K. Toyota, R. Fukuda, J. Hasegawa, M. Ishida, T. Nakajima, Y. Honda, O. Kitao, H. Nakai, M. Klene, X. Li, J. E. Knox, H. P. Hratchian, J. B. Cross, V. Bakken, C. Adamo, J. Jaramillo, R. Gomperts, R. E. Stratmann, O. Yazyev, A. J. Austin, R. Cammi, C. Pomelli, J. W. Ochterski, P. Y. Ayala, K. Morokuma, G. A. Voth, P. Salvador, J. J. Dannenberg, V. G. Zakrzewski, S. Dapprich, A. D. Daniels, M. C. Strain, O. Farkas, D. K. Malick, A. D. Rabuck, K. Raghavachari, J. B. Foresman, J. V. Ortiz, Q. Cui, A. G. Baboul, S. Clifford, J. Cioslowski, B. B. Stefanov, G. Liu, A. Liashenko, P. Piskorz, I. Komaromi, R. L. Martin, D. J. Fox, T. Keith, M. A. Al-Laham, C. Y. Peng, A. Nanayakkara, M. Challacombe, P. M. W. Gill, B. Johnson, W. Chen, M. W. Wong, C. Gonzalez, J. A. Pople, Gaussian, Inc., Wallingford, CT, **2004**.
[50] M. W. Schmidt, K. K. Baldridge, J. A. Boatz, S. T. Elbert, M. Dupuis, J. A. Montgomery, *J. Comput. Chem.* **1993**, *14*, 1347–1363.
[51] M. S. Gordon, M. W. Schmidt, "Advances in Electronic Structure Theory: GAMESS a Decade Later," Theory and Applications of Computational Chemistry" Chapter 41. in: *Theory and Applications of Computational Chemistry: The First Forty Years*, (Eds.: C. E. Dykstra, G. Frenking, K. S. Kim, G. S. Scuseria), Elsevier, Amsterdam, **2005**.
[52] S. Noury, X. Krokidis, F. Fuster, B. Silvi, Universite Pierre et Marie Curie: Paris, **1997**.
[53] A. D. Becke, K. E. Edgecombe, *J. Chem. Phys.* **1990**, *92*, 5397–5403.
[54] A. Savin, R. Nesper, S. Wengert, T. F. Fassler, *Angew. Chem. Int. Ed. Engl.* **1997**, *36*, 1809–1832.
[55] J. R. Gillepsie, *Chem. Soc. Rev.* **1992**, *21*, 59–69.
[56] J. Poater, M. Duran, M. Sola, B. Silvi, *Chem. Rev.* **2005**, *105*, 3911–3947.
[57] Y. Mo, S. D. Peyerimhoff, *J. Chem. Phys.* **1998**, *109*, 1687–1697.
[58] Y. Mo, L. Song, Y. Lin, *J. Phys. Chem. A* **2007**, *111*, 8291–8301.
[59] Y. R. Mo, *Org. Lett.* **2006**, *8*, 535–538.
[60] Y. Mo, Y. Zhang, J. Gao, *J. Am. Chem. Soc.* **1999**, *121*, 5737–5742.
[61] I. G. Csizmadia, A. H. Cowley, M. W. Taylor, L. M. Tel, S. Wolfe, *J. Chem. Soc. Chem. Comm.* **1972**, 1147–1148.
[62] I. G. Csizmadia, A. H. Cowley, M. W. Taylor, S. Wolfe, *J. Chem. Soc. Chem. Comm.* **1974**, 432–433.
[63] M. Barthelat, R. Mathis, J. F. Labarre, F. Mathis, *Comput. Rend.* **1975**, *280*, 645–647.
[64] M. H. Whangbo, S. Wolfe, *Can. J. Chem.* **1976**, *54*, 949–962.
[65] A. H. Cowley, M. W. Taylor, M. H. Whangbo, S. Wolfe, *J. Chem. Soc. Chem. Comm.* **1976**, 838–839.
[66] M. Barthelat, R. Mathis, F. Mathis, *J. Chem. Soc. Chem. Comm.* **1977**, 615–616.
[67] A. H. Cowley, D. J. Mitchell, M. H. Whangbo, S. Wolfe, *J. Am. Chem. Soc.* **1979**, *101*, 5224–5231.
[68] D. Gonbeau, D. Liotard, G. Pfister-Guillouzo, *Nouveau J. de Chimie* **1980**, *4*, 227–233.
[69] A. V. Belyakov, A. Haaland, D. J. Shorokhov, V. I. Sokolov, O. Swang, *J. Mol. Struct.* **1998**, *445*, 303–309.
[70] At the B3LYP/6-311+G(d,p) level.
[71] M. D. Wodrich, C. S. Wannere, Y. Mo, P. D. Jarowski, K. N. Houk, Pv. R. Schleyer, *Chem. Eur. J.* **2007**, *13*, 7731–7744.
[72] D. B. Chesnut, *J. Phys. Chem. A.* **2000**, *104*, 7635–7638.
[73] A. F. Wells, *Structural Inorganic Chemistry*, 5th edn, Oxford University Press, London, **1984**. p. 793.
[74] K. Hedberg, *J. Am. Chem. Soc.* **1955**, *77*, 6491–6492.
[75] B. Beagley, A. R. Conrad, *Trans. Faraday Soc.* **1970**, *66*, 2740–2744.
[76] C. J. Rhodes, *J. Chem. Soc. Perkin Trans.* **1992**, *2*, 235–241.
[77] U. Salzner, Pv. R. Schleyer, *J. Am. Chem. Soc.* **1993**, *115*, 10231–10236.
[78] See e.g., Asymmetric Catalysis Special Feature Part I and Part II. *in PNAS, 101, no 15 and 16*, **2004**.
[79] F. H. Allen, J. E. Davies, J. J. Galloy, O. Johnson, O. Kennard, E. McRae, G. F. Mitchell, J. M. Smith, D. G. Watson, *J. Chem. Inf. Comput. Sci.* **1991**, *31*, 187–204.